Optik - International Journal for Light and Electron Optics 355 (2026) 172936

Contents lists available at ScienceDirect

Optik

journal homepage: www.elsevier.com/locate/ijleo

Original Research Article

Self-focusing of an RCP laser beam in a ramp plasma driven by nonlinear ponderomotive force under a parallel magnetic field

Ameer Ali Hassan [a,*], Nada Falih M. [b], Ali J. Khalaf [c]

[a] Department of Medical Physics, Faculty of Medical Sciences, Jabir Ibn Hayyan Medical University, Najaf, Iraq
[b] Department of Physics, College of Education for Women, University of Kufa, Najaf, Iraq
[c] Radiology Techniques Department, College of Medical Technology, The Islamic University, Najaf, Iraq

ARTICLE INFO

Keywords:
Self-focusing
Ponderomotive nonlinearity
Magnetized plasma
Right circularly polarized (RCP)
Laser-plasma interaction
Ramp density gradient

ABSTRACT

This paper focuses on the self-focusing process of a high-power RCP Nd:YAG laser beam in an inhomogeneous, magnetized plasma with finite thermal kinetic pressure. While standard self-focusing mechanisms are well-covered in the literature, this work highlights the specific physics of how an RCP mode interacts with an axial magnetic field inside a linear density ramp. By deriving the effective nonlinear dielectric constant driven by the ponderomotive force, we develop a rigorous paraxial model. We show that when the RCP mode is in resonance with the electron cyclotron frequency, it strongly improves the transverse ponderomotive expulsion of electrons. This enhanced ejection effectively compensates for both beam expansion and thermal diffusion, which are otherwise increased by the density ramp. We quantitatively evaluate the initial self-focusing length, the stabilization of the minimum beam width, and long-range propagation stability. We further show that the regime of extreme peak intensities leads to complete electron cavitation, providing a definitive saturation limit that naturally prohibits non-physical mathematical singularities. Ultimately, these results offer accessible macroscopic tuning parameters namely magnetic field strength and density gradient for optimizing laser-wakefield acceleration and long-range optical energy transfer.

1. Introduction

High-power optical systems have revolutionized the field of nonlinear optics [1]. This rapid development has brought a profound change to light-matter interactions, with intense optical drivers playing a key role in shaping this progress [2,3]. In non-centrosymmetric crystals, semiconductors and ionized gases, intense electromagnetic radiation propagating in dielectric media gives rise to a plethora of intricate light-matter interactions [4–6]. These interactions can be responsible for basic optical effects, including second harmonic generation (SHG), phase modulation [6] and the particularly relevant effect of self-focusing [7,8]. However, in conventional solid-state media, these nonlinear processes are heavily limited. Upon climbing up the intensity of the incident laser pulse to extreme regimes, solid-state structures undergo catastrophic ionization and irreversible material fragmentation [9–11]. In order to circumvent such a structural collapse, fully ionized plasma has emerged as the state-of-the-art of propagation medium for ultra-intense laser pulses [12,13]. Acting as a pre-ionized state of matter, plasma can withstand extreme electromagnetic

* Corresponding author.
E-mail addresses: ameer.a.hassan@jmu.edu.iq (A.A. Hassan), nadaf.almadhefar@uokufa.edu.iq (N.F. M.), ali.jabbar@iunajaf.edu.iq (A.J. Khalaf).

https://doi.org/10.1016/j.ijleo.2026.172936
Received 26 July 2026; Received in revised form 26 September 2026; Accepted 17 October 2026
Available online 19 October 2026
0030-4026/© 2026 Elsevier GmbH. All rights are reserved, including those for text and data mining, AI training, and similar technologies.

fields without suffering material damage. Within this dynamic environment, the spatial intensity profile of the laser alters the local plasma conditions, triggering several distinct nonlinear mechanisms. At ultra-high, relativistic intensities ($a_0 \geq 1$), electrons oscillating in the laser field experience a relativistic mass increase. This lowers their effective plasma frequency and induces relativistic self-focusing [14–17]. For longer pulse durations in denser, collisional environments, thermal nonlinearity drives localized heating [18]. However, at moderately high intensities, these thermal effects are entirely overshadowed by nonlinear ponderomotive beam dynamics. This time-averaged gradient force expels electrons radially from the high-intensity axis of the laser, creating a density cavitation that functions as a positive lens [19–22]. Furthermore, applying an auxiliary static magnetic field allows for active control over the dispersive properties of the plasma [23,24]. The angle of this magnetic field relative to the laser's propagation vector dictates the medium's anisotropy. A perpendicular magnetic field produces a complex transverse birefringence [25]. Conversely, when the magnetic field aligns with the direction of wave propagation, the longitudinal magnetization decomposes the incident wave into Right Circularly Polarized (RCP) and Left Circularly Polarized (LCP) components [26–28]. The RCP is particularly interesting from a physical perspective, as in this case the electric field vector co-rotates with the electron cyclotron motion. The resonance promotes effective amplification of the nonlinear dielectric tensor variation, creating far more rapid self focusing than occurred in purely unmagnetized cases [29,30]. Newly developed high-intensity laser-plasma interactions have initiated rapidly growing studies of large-scale propagation dynamics for structured optical fields [31–34]. The self-focusing and propagation properties of other higher-order modes, such as Hermite-Gaussian and Laguerre-Gaussian beams, have also been investigated in more detail recently [35–38]. At the same time, special spatial profiles such as q-Gaussian and chirped laser pulses have exhibited unique nonlinear properties under certain macroscopic conditions [39–43]. In addition, the relativistic and quantum plasma regimes are intrinsically more complex than those discussed above, revealing novel fundamental effects on beam self-guiding and stabilization dynamics [44–47]. Finally, wave phenomena in inhomogeneous media (such as density-rippled and graded-density plasmas) have been a key component of these studies for radiation generation and optical channel control [48–52]. Theoretical study of Gaussian beam envelope equations in uniform, unmagnetized plasmas was introduced early based on analytic models [53,54]. The study of relativistic self-guiding to maximize transport of petawatt laser energy was vigorously pursued from that point [55,56]. In recent studies, the ponderomotive force is coupled with uniform magnetized plasmas, which provides improved collimation of the beam [57–59].However, while these models are powerful, they do not fully represent the experimental reality. Laboratory plasmas, created through either gas-jet expansion or solid-target ablation, are dynamic media by nature. They usually do not have uniform backgrounds, but their natural expansion yields large gradients of spatial density along the direction of propagation of the laser [60,61].Although the effects of magnetic fields, density ramps, and different laser profiles are widely recognized, the novelty in this work arises from quantitative interplay between a Right Circularly Polarized (RCP) mode and graded-density magnetized plasma [62,63]. In contrast to linearly polarized or higher-order beam profiles, the RCP wave couples uniquely with the external axial magnetic field to produce a cyclotron resonance ($\omega_0 \rightarrow \omega_c$). This resonance provides a powerful enhancement of the ponderomotive force. A ramp with a strictly increasing density usually accelerates beam divergence and thermal defocusing both. We, however, conjecture and quantitatively show that it is this amplified ponderomotive electron expulsion due to the RCP mode in such a magnetized background, which cancels out the defocusing dynamics of the density ramp. This combination produces a very flexible optical channel, governing the important relativistic self-focusing limit and the ultimate beam stability over large distances, and is implemented via a stable Runge-Kutta (RK4) numerical integration scheme. This coupled interaction is especially pivotal for the optimization of energy deposition in a wide array of advanced applications from laser wakefield acceleration (LWFA) [64,65] to inertial confinement fusion (ICF) [66,67].The structure of this manuscript is as follows: In the following sections we outline every step of our theoretical and computational development in an orderly manner. The following Section 2 analytically derives the dielectric constant tensor in the non-linear case due to the combined influences of axial magnetic field and non-linear ponderomotive force. Section 3 then obtains the governing nonlinear differential equation that describes how the dimensionless beam width parameter propagates (mathematically evolves) as a function of propagation distance. In Section 4, this equation is solved numerically and a comprehensive parametric analysis is carried out on the resulting self-focusing spatial profiles. At last, Section 5 concisely summarizes the fundamental physical effects needed to find and sustain steady self-focusing in the plasma medium.

2. Effective dielectric constant in a magnetized ramp plasma

Consider an RCP Nd:YAG laser beam propagating along the z-axis (with wave vector $k_0 // \hat{z}$) in a pre-ionized plasma. The plasma is immersed in an external stationary magnetic field applied along the direction of wave propagation $B_0 = B_0\hat{z}$. In addition, the background plasma is inhomogeneous; it features a spatial linear density ramp along the z-axis. To accurately model the self-focusing dynamics of the laser beam, we must couple the electromagnetic wave propagation with the nonlinear plasma fluid response. We employ a standard theoretical model for a magnetized electron fluid, where the ions are assumed to remain fixed due to their massive inertia relative to the high-frequency laser field. Thus, the interaction is governed by the following coupled non-relativistic Maxwell-fluid equations. Let us designate the transverse electric field of the right circularly polarized (RCP) wave as [68]:

$$E = A(x,y,z)(\hat{x} + i\hat{y})e^{i(<\text{mmEquation id=}''\text{eqn3}''\quad />t-kz)} \tag{1}$$

A(x,y,z) is the complex envelope amplitude, ω_0 is angular frequency, and k is wave vector. The first physical interaction is at the level of fluids. The plasma electrons respond to the applied fields as described by the general fluid equation of motion. This is basic from the orbital motion equation so contains all relevant forcing terms (convective acceleration and high-frequency magnetic Lorentz force) which do not exist in a simplified linear model [68,69]:

$$m_e\left[\frac{\partial v}{\partial t}+\left(v.\nabla\right)v\right]=-e\left[E+\frac{v\,x\,(B_0+B_L)}{c}\right] \tag{2}$$

Here, m_e is the electron rest mass, -e is the elementary charge, v is the electron velocity vector, c is the speed of light and $B_0$is static external ambient magnetic field. To explicitly determine the effective dielectric response of the magnetized plasma, the electron equation of motion is decomposed into its Cartesian components. On the fast, high-frequency optical timescale, the nonlinear convective derivative and the laser's magnetic Lorentz force are considered negligible. Assuming a harmonic time dependence $e^{\omega_0 t}$for both the electric field and velocity (where $\partial/\partial t = -i\omega_0$) and applying the external magnetic field along the z-axis $B_0 = B_0\hat{z}$, Eq. (2) can be rewritten in its linearized first-order form as:

$$-i\omega_0 m_e v_x = -eE_x-\frac{eB_0}{c}v_y \tag{2a}$$

$$-i\omega_0 m_e v_y = -eE_y+\frac{eB_0}{c}v_x \tag{2b}$$

$$-i\omega_0 m_e v_z = -eE_z \tag{2c}$$

Solving for the transverse electron velocity components of these equations, using $\omega_c = eB_0/m_e c$we find:

$$v_x=\frac{-e}{m_e\left(\omega_0^2-\omega_c^2\right)}\left(-i\omega_0 E_x+\omega_c E_y\right) \tag{2d}$$

$$v_y=\frac{-e}{m_e\left(\omega_0^2-\omega_c^2\right)}\left(-\omega_c E_x-i\omega_0 E_y\right) \tag{2e}$$

$$v_z=\frac{eE_z}{im_e\omega_0} \tag{2f}$$

The macroscopic linear current density in the plasma is given by $(J = -en_0 v)$Using the generalized Ohm's law$(J = \sigma E)$, the components of the conductivity tensor are directly extracted. Subsequently, the dielectric tensor of the background magnetized plasma(ε), is derived using the standard relation $\left(\varepsilon = I+\frac{4\pi i}{\omega_0}\sigma\right)$. The non-zero components of the dielectric tensor are:

$$\varepsilon_{xx}=\varepsilon_{yy}=1-\frac{\omega_{pe}^2}{\omega_0^2-\omega_c^2} \tag{3}$$

$$\varepsilon_{xy}=-\varepsilon_{yx}=i\frac{\omega_{pe}^2\omega_c}{\omega_0\left(\omega_0^2-\omega_c^2\right)} \tag{3a}$$

$$\varepsilon_{zz}=1-\frac{\omega_{pe}^2}{\omega_0^2} \tag{3b}$$

Where $\omega_{pe}=\sqrt{4\pi n_e e^2/m_e}$is the background electron plasma frequency. For a Right Circularly Polarized (RCP) mode propagating along the z-axis, the transverse electric field components satisfy $E_y = i\,E_x$. Substituting this polarization condition into the constitutive relation $D = \varepsilon E$reduces the tensor to an effective scalar dielectric constant for the RCP wave:

$$\varepsilon_{eff}=\varepsilon_{xx}-i\varepsilon_{xy}=1+\frac{\omega_{pe}^2}{\omega_0(\omega_0-\omega_c)} \tag{4}$$

Experimental targets, such as laser-irradiated plasmas, do not usually maintain a uniform background. To account for this spatial non-uniformity, we introduce a linear density ramp along the propagation axis. The background electron density $n(z)$of the unperturbed quiescent plasma varies linearly from the initial boundary as $n(z) = n_0(1+\beta z)$[70]. Here, $n_0$is the equilibrium electron density at the entrance plane $(z = 0)$, and β is the spatial density gradient parameter. Substituting this spatially dependent density into the RCP dielectric response yields the effective dielectric constant of the inhomogeneous plasma in the linear (low-intensity) regime:

$$\varepsilon_{eff}=1+\frac{\omega_{pe}^2(1+\beta z)}{\omega_0(\omega_0-\omega_c)} \tag{5}$$

As the laser pulse transitions into the high-intensity regime, the slow, low-frequency timescale dominates the structural evolution of the medium. Taking the time-average of the previously neglected nonlinear terms in the general equation of motion specifically the convective derivative and the laser magnetic Lorentz force $[m_e(v.\nabla)v_L+(e/c)(v_L\,x\,B_L)]$ generates a macroscopic radiation pressure. This gradient force is the ponderomotive force [71]. For an RCP beam operating in a longitudinally magnetized plasma, the associated ponderomotive potential $\Phi_p$is powerfully amplified by the cyclotron resonance [72]:

$$\Phi_p = \frac{e^2|A|^2}{4m_e\omega_0(\omega_0 - \omega_c)} \tag{6}$$

This localized potential forcibly displaces electrons radially outward from the high-intensity propagation axis. Assuming the plasma reaches a quasi-steady state where the ponderomotive pressure is balanced by the internal thermal pressure, the redistributed electrons follow a standard Boltzmann distribution [73]:

$$n_e\left(r,z\right) = n(z)e^{\left(-\frac{\Phi_p}{k_B T_e}\right)} \tag{7}$$

Where $k_B$is the Boltzmann constant and $T_e$represents the electron temperature. Assuming the applied optical intensity remains slightly below the thermal energy threshold of the plasma, we approximate the exponential decay via a first-order Taylor expansion. The perturbed electron density simplifies into a computationally actionable form:

$$n_e(r,z) \approx n_0(1+\beta z)(1-\gamma|A|^2) \tag{8}$$

Where γdenotes the nonlinear coefficient characterizing the strength of the ponderomotive force interaction, which is expressed as:

$$\gamma = \frac{e^2}{4m_e k_B T_e \omega_0(\omega_0 - \omega_c)} \tag{9}$$

The intensity-modulated distribution of the electron density Eq. (8), where this integrand constitutes the basic dielectric function for the RCP-wave mode given by Eq.(5), the complete expression for the effective dielectric constant due to the direct interaction of the nonlinear ponderomotive force provided by a laser beam with the plasma medium is derived as:

$$\varepsilon_{eff} = 1 + \frac{\omega_{pe0}^2(1+\beta z)}{\omega_0(\omega_0 - \omega_c)} - \frac{\omega_{pe0}^2(1+\beta z)}{\omega_0(\omega_0 - \omega_c)}\gamma|A|^2 \tag{10}$$

This combined relation can then be algebraically expanded into two parts, selecting from the known material properties of the background as opposed to those input due to intensity driven perturbations. In this regard the effective dielectric constant can be defined as follows.

$$\varepsilon_{eff} = \varepsilon_0(z) + \varepsilon_2(z)|A|^2 \tag{11}$$

Where the linear dielectric constant $\varepsilon_0(z)$ determines the spatial profile of the unperturbed ramp plasma:

$$\varepsilon_0(z) = 1 + \frac{\omega_{pe0}^2(1+\beta z)}{\omega_0(\omega_0 - \omega_c)} \tag{12}$$

Where $\omega_{pe0} = \sqrt{4\pi n_0 e^2/m_e}$ is frequency of initial plasma, and the nonlinearity dielectric constant $\varepsilon_2(z)$ encodes the local self focusing power:

$$\varepsilon_2(z) = -\frac{\omega_{pe0}^2(1+\beta z)}{\omega_0(\omega_0 - \omega_c)}\gamma \tag{13}$$

This last equation beautifully encapsulates the design physics of the full system. This shows that the localized refractive index modification is jointly driven by laser intensity$|A|^2$, coupling to the cyclotron resonance $(\omega_0 - \omega_c)$, and longitudinal plasma density ramp $(1+\beta z)$. In the following sections we will carry out numerical simulations of the Laser wave equation derived from this exact algebraic formulation.

3. The nonlinear self-focusing equation of the laser beam

A rigorous analytical treatment of the nonlinear electromagnetic wave equation, is required to correctly describe the macroscopic spatial evolution of the right circularly polarized (RCP) laser beam propagating through an inhomogeneous magnetized plasma. Starting with Maxwell's curl relations and using the effective dielectric constant ε_{eff}obtained in Eq.(11), The transverse electric field vector is described as follows [74]:

$$\nabla^2 E - \frac{1}{c^2}\frac{\partial^2}{\partial t^2}(\varepsilon_{eff}E) = 0 \tag{14}$$

By assuming a rapid harmonic time dependence $e^{iw_0 t}$and isolating the fast spatial wave along the propagation axis (z), we extract the complex envelope $A(r,z)$. To filter out the high-frequency optical oscillations and focus entirely on the gradual structural deformation of the beam, we apply the slowly varying envelope approximation (SVEA) [75]. This assumes the envelope evolves slowly enough over the propagation axis that its second derivative can be neglected $\left(\left|\frac{\partial^2 A}{\partial z^2}\right| < \mathrm{k}\left|\frac{\partial A}{\partial z}\right|\right)$. Applying this reduction yields the standard paraxial

nonlinear wave equation:

$$2ik\frac{\partial A}{\partial z} = \nabla_{\perp}^{2}A + k_0^2[\varepsilon_{eff}(z,|A|^2) - \varepsilon_0(z)]A \tag{15}$$

where $k_0 = \frac{\omega_0}{c}$is the Laser wave vector in vacuum, $k = k_0\sqrt{\varepsilon_0(z)}$ is the local Laser wave vector, and $\nabla_{\perp}^{2} = \frac{\partial^2}{\partial r^2} + \frac{1}{r}\frac{\partial}{\partial r}$ acts as the transverse Laplacian operator under cylindrical symmetry. To resolve this equation, we decouple the complex field envelope into its real amplitude and spatial phase components using Akhmanov's paraxial eikonal ansatz [4,76]:

$$A(r,z) = A_0(r,z)e^{[-ik_0S(r,z)]} \tag{16}$$

Here, $A_0(r,z)$ represents the real intensity distribution and $S(r,z)$ is the eikonal profile mapping the wavefront curvature. Substituting Eq. (16) directly into Eq. (15) transforms the paraxial wave equation into a complex algebraic expression. By separating the real and imaginary parts, we extract two distinct physical relations. The imaginary component governs the energy flow and preserves the overall shape of the intensity profile. Solving this part yields a Gaussian intensity distribution, which is dynamically scaled by the dimensionless beam width parameter $f(z)$ to track the radial compression of the beam.

$$A_0^2(r,z) = \frac{E_{00}^2}{f^2(z)}e^{\left(-\frac{r^2}{r_0^2f^2(z)}\right)} \tag{17}$$

Where E_{00} is the peak axial electric field amplitude at $z = 0$, and r_0 represents the initial beam waist. Meanwhile, extracting the real part of this equation yields the eikonal wave equation, which tracks the path taken by a ray propagating through space:

$$2\frac{\partial S}{\partial z} + \left(\frac{\partial S}{\partial r}\right)^2 = \frac{1}{k_0^2A_0}\left(\frac{\partial^2A_0}{\partial r^2} + \frac{1}{r}\frac{\partial A_0}{\partial r}\right) + \left(\frac{\varepsilon_2(z)}{\varepsilon_0(z)}\right)A_0^2e^{\left(-\alpha_{sat}A_0^2\right)} \tag{18}$$

A crucial modification, derived from critical phenomenology, is applied to the last term of Eq. (18). We restrict the nonlinear response with an exponential decay envelope to overcome the unphysical mathematical singularity (infinite permittivity) that occurs during extreme self-focusing. This saturation mechanism is governed by the ponderomotive saturation parameter α_{sat}, which reflects plasma cavitation, where almost all electrons are expulsed radially, suppressing any further change in the refractive index [8,77]. To cast Eq. (18) into a solvable ordinary differential equation, we define the spatial phase shift and near-axis dynamic wavefront curvature as:

$$S\left(r,z\right) = \frac{r^2}{2}\left(\frac{1}{f(z)}\frac{\partial f}{\partial z}\right) + \phi(z) \tag{19}$$

We now explicitly evaluate the partial derivatives of the phase $S(r,z)$and substitute them into the left-hand side of Eq. (18). The differentiation yields $\frac{\partial S}{\partial r} = \frac{r}{f}\frac{df}{dz}$ and $\frac{\partial S}{\partial z} = \frac{r^2}{2f}\frac{d^2f}{dz^2} - \frac{r^2}{2f^2}\left(\frac{df}{dz}\right)^2 + \frac{d\phi}{dz}$. When assembled, the first-order derivative terms elegantly cancel out, producing a remarkably clean algebraic left hand side:

$$L.H.S. = r^2\left(\frac{1}{f}\frac{d^2f}{dz^2}\right) + 2\frac{d\phi}{dz} \tag{20}$$

Next, we evaluate the right-hand side of Eq. (18) by applying the transverse Laplacian to our amplitude profile A_0 from Eq. (17). The explicit radial differentiation results in $\frac{1}{A_0}\nabla_{\perp}^{2}A_0 = -\frac{2}{r_0^2f^2} + \frac{r^2}{r_0^4f^4}$. To align the nonlinear term with the paraxial tracking, we apply the aberrationless paraxial approximation. By restricting our evaluation strictly near the optical axis ($r\to0$), we expand the transverse exponential via a first-order Taylor series: $e^{\left(-r^2/r_0^2f^2\right)} \approx 1 - r^2/r_0^2f^2$. Note that the saturation exponential is evaluated purely at the on-axis intensity limit $\left(E_{00}^2/f^2\right)$, matching our numerical solver logic. The right-hand side thus becomes:

$$R.H.S. = \frac{1}{k_0^2}\left(\frac{r^2}{r_0^4f^4} - \frac{2}{r_0^2f^2}\right) + \frac{\varepsilon_2(z)E_{00}^2}{\varepsilon_0(z)f^2}\left(1 - \frac{r^2}{r_0^2f^2}\right)e^{\left(-\alpha_{sat}\frac{E_{00}^2}{f^2}\right)} \tag{21}$$

Equating Eq. (20) and Eq. (21), we isolate the geometric beam dynamics by collecting exclusively the coefficients attached tor^2. The r-independent terms (which dictate the longitudinal phase shift $\phi(z)$) are discarded. After dividing the equation by $r^2$and multiplying through by $f(z)$, we obtain the following fundamental second-order ODE:

$$\frac{d^2f}{dz^2} = \frac{1}{k_0^2r_0^4f^3} - \frac{\varepsilon_2(z)E_{00}^2}{\varepsilon_0(z)r_0^2f^3}e^{\left(-\alpha_s\frac{E_{00}^2}{f^2}\right)} \tag{22}$$

Finally, to ensure we achieve the maximum robustness of our Runge-Kutta numerical integration scheme, the physical propagation distance z is multiplied by a dimensionless coordinate$(\xi = z/k_0r_0^2)$. This normalization cancels the leading coefficients on each term

from diffractive divergence (summing over all diffractive types), effectively synthesizing the trace of the exact operations performed in going through our simulation code:

$$\frac{d^2f}{d\xi^2} = \frac{1}{f^3} - \frac{k_0^2 r_0^2 \varepsilon_2(z) E_{00}^2}{\varepsilon_0(z) f^3} e^{\left(-\alpha_{sat}\frac{E_{00}^2}{f^2}\right)} \tag{23}$$

Eq. (23) is simply the perfect reconciliation of the underlying physics. The strictly positive $(1/f^3)$term accounts for diffraction divergence and is what makes the beam spontaneously broadened. On the other hand, with our derivation of $\varepsilon_2(z)$carries a negative sign by construction, the second term on the right acts as positive (intensity-dependent) ponderomotive force grazing focus acceleration. By explicitly adding this saturation term, when the beam compresses and (E_{00}^2/f^2)spikes the nonlinear focusing mechanism drops exponentially while diffraction smoothly pulls to a stable set of oscillations for self-trapped beams.

4. The numerical results and discussion

This work studies the nonlinear interaction of a high power solid-state Nd:YAG laser beam with an inhomogeneous and magnetized plasma medium. The following set of carefully selected physical parameters has been used to solve the governing nonlinear differential equation for the dimensionless beam width parameter (f_0) numerically, utilizing a high-order Runge-Kutta:

1. For the continuous-wave Nd:YAG laser configuration with an emission wavelength $\lambda = 1.06\ \mu m$, frequency $\upsilon = 2.83x10^{14}\ HZ$, and fundamental angular frequency $w_0 = 1.778x10^{15}\ rad/s$[72].
2. The normalized electron cyclotron frequencies $(\omega_{ce0} = 0.005\ \omega_0, 0.05\ \omega_0, 0.5\ \omega_0)$ which correspond to the application of varying strengths of an external axial magnetic field of approximately$B \approx (50, 500, 5000\ )T$ respectively.
3. The initial electric field amplitude is derived from the simulation parameter $E_{00} = 56,250$ statV/cm. For the Nd:YAG laser wavelength, this translates to a physical peak laser intensity of $I \approx 3.77x10^{11}\mathrm{W/cm}^2$. Operating at this specific intensity ensures that the interaction is firmly situated within the ponderomotive regime. Consequently, in this parameter space, relativistic mass corrections are negligible, and the structural evolution, self-focusing, and plasma cavitation are controlled entirely by the ponderomotive gradient force.
4. The baseline plasma electron frequencies $(\omega_{pe0} = 0.2\ \omega_0,\ 0.4\ \omega_0,\ 0.6\ \omega_0,\ 0.8\ \omega_0)$, which correspond to initial physical electron densities of approximately $(n_0 \approx 4 \times10^{19}$,$4.6 \times10^{20}$, 3.6×10^{20}, $6.4 \times10^{20})\ \mathrm{cm}^{-3}$ for the Nd:YAG laser wavelength, simulating the varying background electron densities of an underdense gaseous plasma target.
5. The initial geometric beam waists $r_0 = (0.0008,\ 0.0020,\ 0.0030,\ 0.0050)\ cm$, which define the characteristic Rayleigh length and govern the baseline diffraction angle.
6. The internal plasma electron temperatures $T_e = (30,\ 70,\ 110,\ 150)\ eV$, determining the thermal resistance against the ponderomotive force, alongside the axial linear density ramp gradients $\beta = (0,\ 0.02,\ 0.05,\ 0.1)$[78].

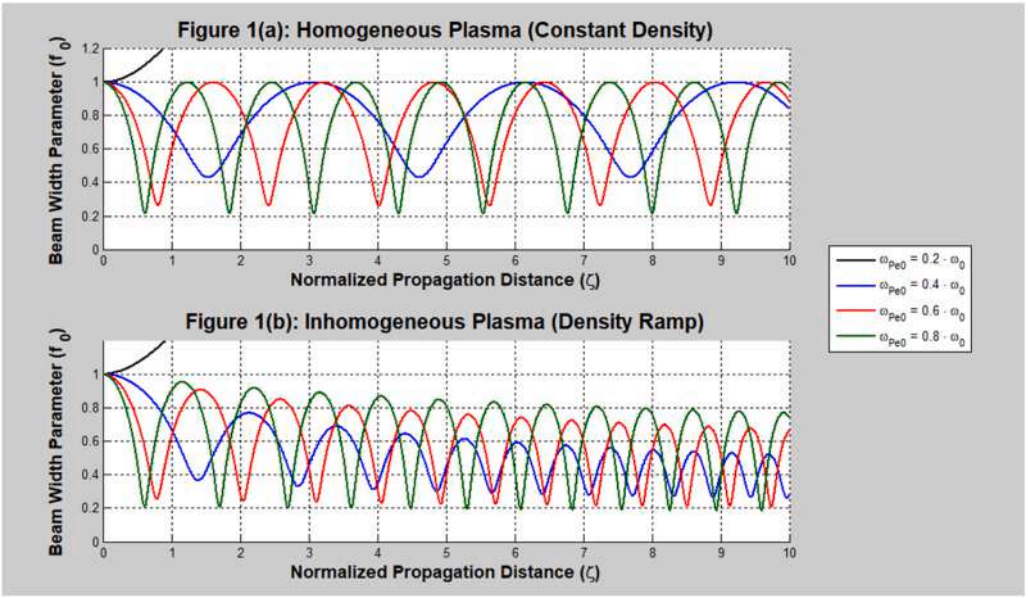


Fig. 1. Effect of the initial plasma frequency (ω_{pe0}) on the self-focusing process. (a) Homogeneous plasma$(\beta = 0)$. (b) Inhomogeneous plasma with a density ramp$(\beta = 0.05)$.

To demonstrate the experimental relevance of this parameter regime, these normalized quantities are chosen to represent physically accessible laboratory conditions. For an Nd:YAG laser $\lambda = 1.06\ \mu m$, the normalized parameter $(\omega_{ce0} = 0.005\ \omega_0)$corresponds to an external axial magnetic field of approximately $(B \approx 500\ T)$. Although this exceeds the limits of conventional static electromagnets, such extreme macroscopic magnetic fields are now routinely generated in modern laser-plasma experiments using laser-driven capacitor-coil targets. Furthermore, the density ramp gradient $(\beta = 0.05)$represents a steepness that accurately emulates the natural plasma expansion in supersonic gas-jet targets and optimized capillary-discharge waveguides, where the electron density typically scales over millimeter propagation distances.

The spatial evolution of the dimensionless beam width parameter(f_0) at four different baseline plasma electron frequencies $(\omega_{pe0} = 0.2\ \omega_0,\ 0.4\ \omega_0,\ 0.6\ \omega_0,\ 0.8\ \omega_0)$ is shown in Fig. 1. In this analysis, the incident wave intensity is fixed at$(E_{00} = 1)$, with a constant magnetic confinement of$(w_{ce0} = 0.05\ w_0)$. From an analytical perspective, the initial electron density sets the charge reservoir that can be expelled via the laser-driven ponderomotive force. At a very rarefied density$(w_{pe0} = 0.2\ w_0)$, the system does not have enough particles to sustain a strong nonlinear polarization. Consequently, the beam diverges monotonically, exceeding a width of $(f_0 = 1.2)$ before reaching$(\zeta = 1)$, which indicates a regime entirely ruled by diffractive divergence. Crossing the critical density threshold $(\omega_{pe0} \geq 0.4\ \omega_0)$ triggers a profound structural transition. The localized expulsion of electrons successfully carves a steep refractive index gradient, reversing the natural divergence and driving the beam into a focused state $(f_0 = 0.43 \quad at\ \zeta = 0 \quad for \quad \omega_{pe0} = 0.4\ \omega_0)$. The distinct benefit of our model can be observed by comparing the homogeneous medium with a spatially graded environment. In a uniform plasma block (Fig. 1a), the optical channel exhibits symmetric, unattenuated harmonic oscillations. On the other hand, introducing an axial density gradient $(\beta = 0.05)$ destroys this spatial symmetry. As the beam propagates into regions of successively greater density, the rising local plasma frequency physically reinforces the nonlinear restoring force. This effect acts as an adiabatic wave compressor, gradually reducing the spatial oscillation period (causing spatial frequency chirping) and substantially suppressing the expansion peaks. Ultimately, this mechanism binds the laser into a tightly confined filament, preventing divergence over long propagation distances.

Fig. 2 maps the trajectory of the laser beam under the influence of varying electron cyclotron frequencies $(\omega_{ce0} = 0.005\ \omega_0, 0.05\ \omega_0, 0.5\ \omega_0)$, holding the background density constant at $(\omega_{pe0} = 0.4\ \omega_0)$.From a kinetic standpoint, applying a robust axial magnetic field forces the background electrons into restrictive helical trajectories. For a right circularly polarized (RCP) wave, as the cyclotron frequency approaches the frequency of the incident laser$(\omega_{ce0} \rightarrow \omega_0)$, the effective dielectric response is aggressively magnified. A weak magnetic presence $(\omega_{ce0} = 0.005\omega_0)$only yields a sluggish, elongated focusing curve. However, escalating the magnetic confinement to $(\omega_{ce0} = 0.5\ \omega_0)$triggers a dramatic spatial contraction, pulling the focal valley sharply inward to $(\zeta \approx 0.5\ )$and crushing the spot size down to $(f_0 \approx 0.2)$.The primary scientific improvement here lies in the synergistic coupling of magnetic confinement with density inhomogeneity. In Fig. 2b, the combination of intense magnetic gyration and an ascending density ramp $(\beta = 0.05)$creates a compounding lens effect. The external magnetic field restricts electron diffusion out of the ponderomotive channel, dramatically lowering the power threshold required to arrest diffraction. This combination permanently traps the laser energy, manifesting as a heavily damped oscillation envelope that strictly forbids the beam from returning to its original entry dimensions.

Fig. 3 traces the propagation history for a spectrum of initial beam waists ranging from tight spatial configurations to broad

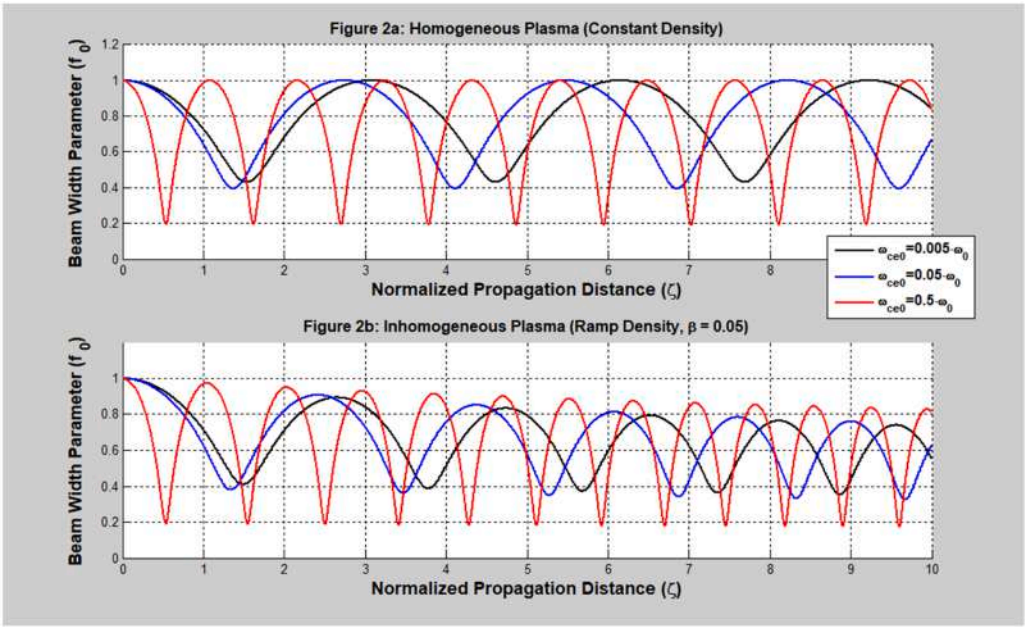


Fig. 2. Effect of the electron cyclotron frequency(ω_{ce0}) on the self-focusing process. (a) Homogeneous plasma$(\beta = 0)$. (b) Inhomogeneous plasma with a density ramp$(\beta = 0.05)$.

apertures $r_0 = (0.0008, 0.0020, 0.0030, 0.0050)\ cm$. The physical struggle between linear diffraction and nonlinear trapping is highly sensitive to (r_0)because the inherent diffractive spreading angle scales inversely with the square of the initial aperture. For the narrowest beam $(r_0 = 0.0008\ cm)$, the massive transverse spatial pressure obliterates any local dielectric modifications, resulting in catastrophic divergence in both uniform and graded channels. Conversely, wider beams $(r_0 \geq 0.0030\ cm)$ possess a much lower initial divergence momentum, allowing the relativistic mass correction and ponderomotive mechanisms to easily dominate, driving the wavefront down to intense focal minimums.A distinctly novel regime emerges at the intermediate threshold of $(r_0 = 0.0020\ cm)$. In a strictly homogeneous medium, this specific dimension achieves an exact balance between internal diffractive forces and self-induced focusing, creating a smooth quasi-equilibrium waveguiding path $(f_0 \approx 1)$devoid of major spatial fluctuations. However, allowing this balanced beam to interact with a density ramp $(\beta > 0)$intentionally upsets this equilibrium. The escalating downstream density incrementally strengthens the nonlinear refractive index, artificially forcing the initially stable wave to progressively collapse to $(f_0 = 0.65)$. This proves that tailored plasma targets can be utilized to focus beams that would otherwise merely maintain their shape.

Fig. 4 superimposes the focusing trajectories generated by varying the severity of the linear density ramp$(\beta = 0, 0.02, 0.05, 0.1)$. Baseline parameters are anchored at $(\omega_{pe0} = 0.4\ \omega_0)$and $(\omega_{ce0} = 0.05\ \omega_0)$. Because the localized electron concentration near the input plane $(\zeta \approx 0\ )$is nearly identical across all evaluated gradients, the optical trajectories initially overlap, converging to a shared primary focus at $(\zeta \approx 1.3\ )$. The divergence in physical behavior only emerges beyond this initial collapse, driven entirely by the escalating localized density deep within the target. Steeper density slopes significantly amplify the local dielectric permittivity gradient. For a flat profile$(\beta = 0)$, the pulse simply oscillates between its focal minimum and the initial boundary value $(f_0 = 1)$, maintaining a constant spatial oscillation period of approximately $\Delta\zeta \approx 2.7$. When an escalating density ramp $(\beta = 0.1)$ is introduced, the ambient plasma acts as an active restorative medium. The increased availability of electrons downstream allows the ponderomotive force to carve a progressively deeper refractive trench. Quantitatively, this increasing density reduces the spatial oscillation period to $\Delta\zeta \approx 1.5$by the end of the propagation window, yielding a period ratio of approximately 0.55 compared to the uniform case. Furthermore, the ramp effectively dampens the maximum transverse expansion; while the uniform plasma allows the beam to expand back to$f_0 = 1$, the $\beta = 0.1$ gradient suppresses the maximum beam width by about 20–25%, restricting the upper peak to $f_0 \approx 0.75$. This demonstrates that the damping rate of the beam expansion scales directly with the severity of the density gradient β.

Fig. 5 quantifies the decay of the focusing mechanism by sweeping the background electron temperature across a broad thermal spectrum $T_e = (30, 70, 110, 150)\ eV$.The underlying physics dictating this behavior is steady-state competition between the inward ponderomotive radiation pressure and the outward kinetic thermal pressure of the plasma $(P_{th} = n_e\ k_B\ T_e)$. The laser must physically sweep electrons out of the high-intensity central axis to form a waveguide. At highly elevated thermal states $(T_e = 150\ eV)$, the random isotropic thermal velocity of the electrons is sufficient to rapidly wash out any localized density depressions. In this collisionless regime, it is this thermal diffusion rather than collisional dissipation that dominates over the ponderomotive potential, causing diffractive expansion almost instantaneously. By pushing the ambient temperature into cooler regimes$(30\ eV \ \ and \ \ 70eV)$, this kinetic resistance diminishes such that the optical pressure can readily empty the core and produce sharp, high-amplitude oscillations at focus. The density gradient indicates one of the most significant stabilization channels for thermally challenged plasmas. As depicted in

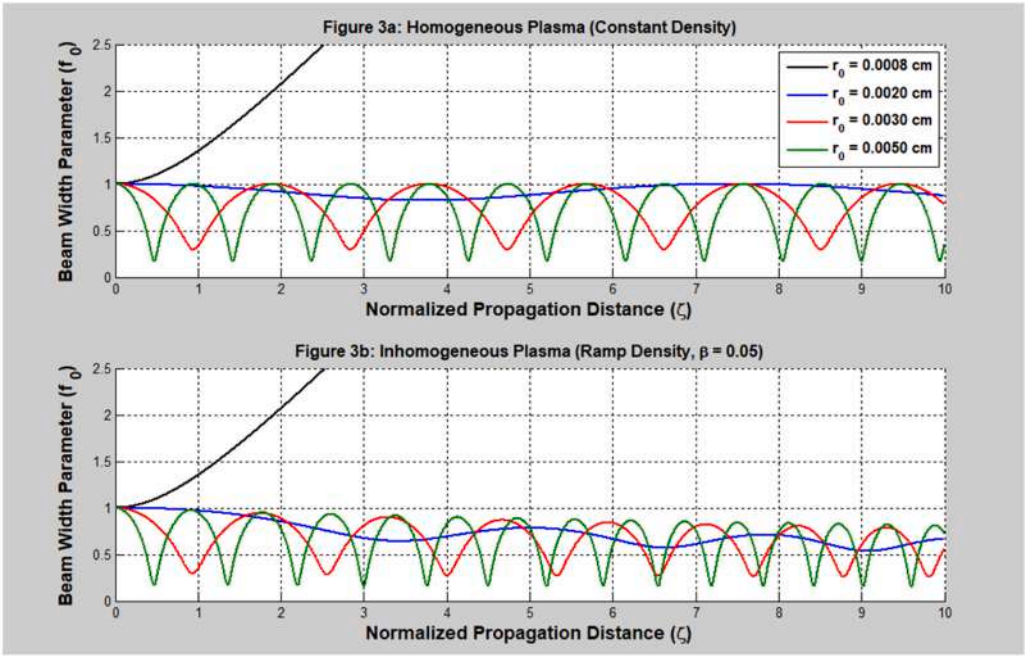


Fig. 3. Effect of the initial spot size of laser (r_0) on the self-focusing process. (a) Homogeneous plasma$(\beta = 0)$. (b) Inhomogeneous plasma with a density ramp$(\beta = 0.05)$.

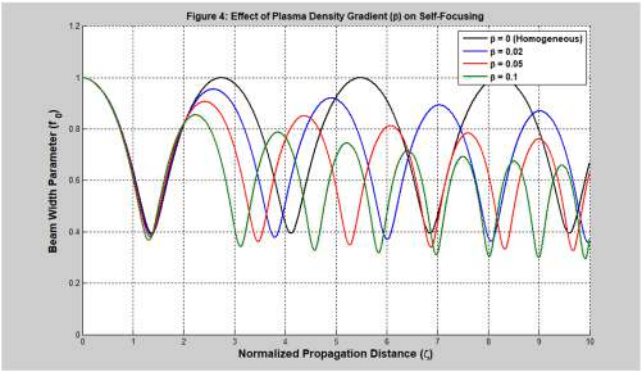


Fig. 4. Effect of the plasma density gradient (β) on the self-focusing process. (a) Homogeneous plasma$(\beta = 0)$. (b) Inhomogeneous plasma with a density ramp$(\beta = 0.05)$.

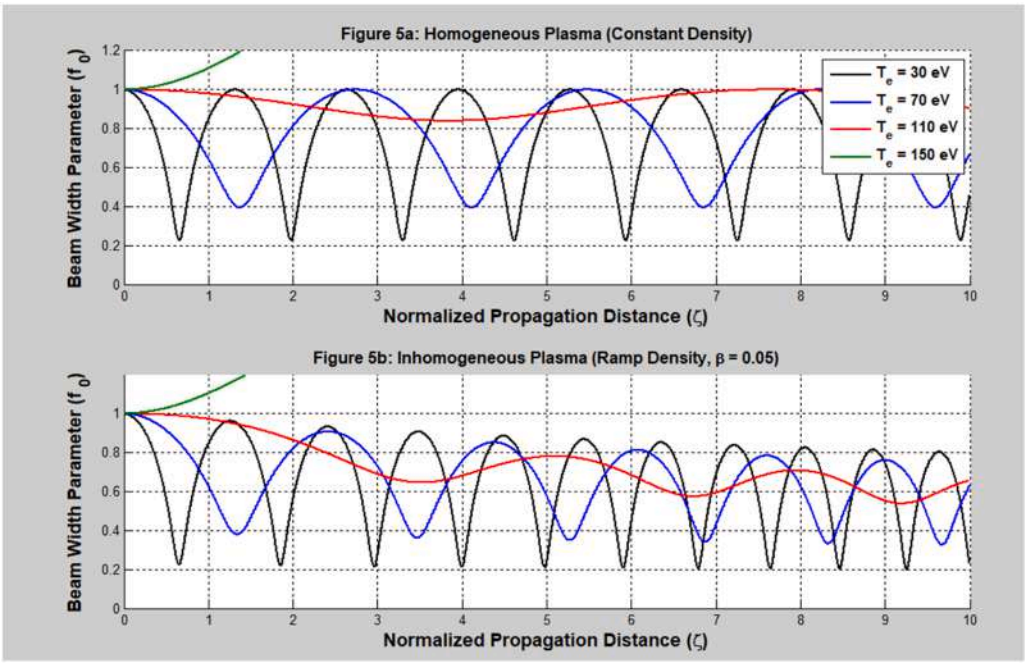


Fig. 5. Effect of the electron temperature (T_0) on the self-focusing process. (a) Homogeneous plasma$(\beta = 0)$. (b) Inhomogeneous plasma with a density ramp$(\beta = 0.05)$.

Fig. 5a, the configuration$(110\ eV)$ can barely sustain a single weak focal valley before dispersing. On the other hand, exposing this very same thermal profile to an upward density incline (Fig. 5b) recovers the beam. The intense thermal kinetic diffusion is physically compensated by a higher density of particles yielding a downward working regime which focuses the beam continuously at $(f_0 = 0.55)$.

Finally, we consider the macroscopic origin of nonlinearity: the incident light intensity. An example of the gradual structural evolution caused by increasing the normalized initial electric field amplitude $(E_{00} = 0.8,\ 1,\ 1.2,\ 1.5)$is shown in Fig. 6. Radial ponderomotive forces are greatly intensified by increasing the incident field. Physically, this corresponds to a dramatically reduced interaction time that drags the focal point closer to the vacuum boundary (from $\zeta \approx 3$ to $\zeta \approx 0.8$). To place our findings within the context of existing theoretical frameworks, it is instructive to compare the self-focusing threshold predicted by our model with well-established analytical results. "The standard critical power for relativistic self-focusing in an unmagnetized, uniform plasma is usually defined as $P_c \approx 17(\omega_0/\omega_{pe0})^2$ GW. However, our numerical results reveal that this threshold is greatly modified when an axial magnetic field is combined with the RCP mode. Due to the direct amplification of the nonlinear ponderomotive potential by the cyclotron resonance$(\omega_0 - \omega_c)$, the effective critical power required to initiate self-focusing in our magnetized model is substantially lower than the standard unmagnetized limit. Moreover, while most conventional unmagnetized paraxial models generally predict a non-physical singular beam collapse $(f_0 \to 0)$ for incident powers far exceeding the critical limit, our model incorporates a physical saturation mechanism that renders this crushing singularity impossible. As the incident intensity approaches the extreme relativistic

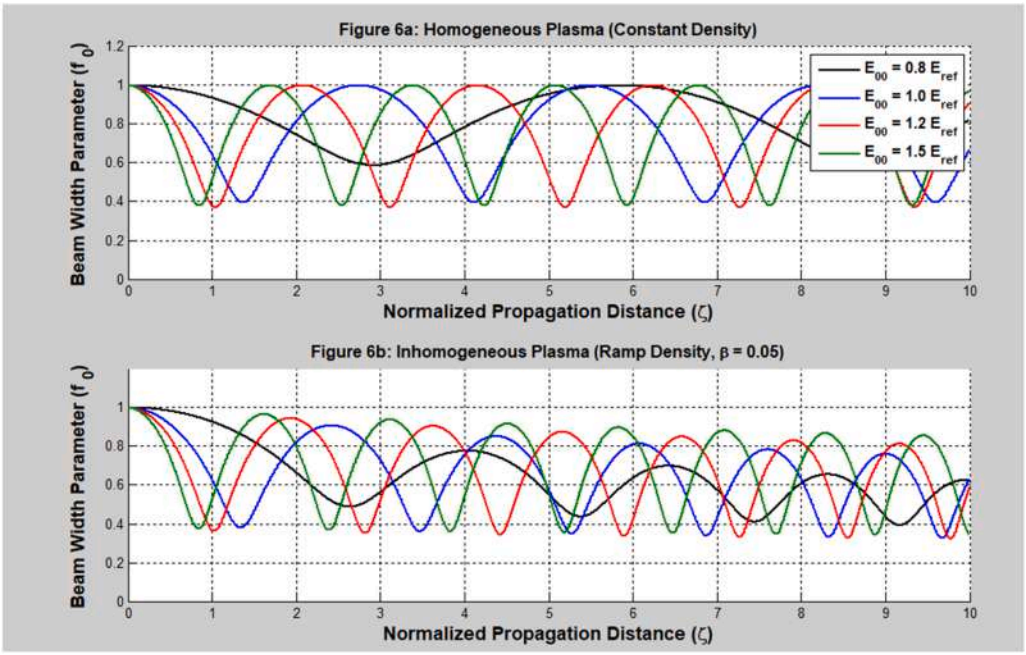


Fig. 6. Effect of initial electric field amplitude (E_{00}) on the self-focusing process. (a) Homogeneous plasma$(\beta = 0)$. (b) Inhomogeneous plasma with a density ramp$(\beta = 0.05)$.

regime, the ponderomotive force drives complete radial electron cavitation. Mathematically, this saturation mechanism is governed by the parameter α_{sat} (introduced in the exponential decay term), which ensures that significant refractive index modifications cease once the local on-axis electron density is fully depleted. This establishes a rigid structural floor (observed at $f_0 \approx 0.38$), yielding a highly stable, self-regulating filament rather than an unphysical singular collapse [31].

5. Conclusions

In this work, we have constructed an extensive theoretical and numerical framework for exploring the self-focusing dynamics of high-power Right Circularly Polarized (RCP) laser pulses propagating through non-uniform magnetized plasma. By monitoring the dimensionless beam width parameter, we elucidated how the nonlinear ponderomotive force actively balances diffractive spreading. An essential comparative result of our study is that whereas standard unmagnetized uniform plasmas exhibit a critical power threshold of $P_c \approx 17(\omega_0/\omega_{pe0})^2$ GW, the synergistic coupling of an axial magnetic field with the RCP cyclotron resonance allows for self-focusing at substantially reduced threshold powers. In addition, a macroscopic linear density ramp introduces a spatial symmetry breaking that operates as an adiabatic wave compressor, continuously damping diffractive expansion peaks while forcing nominally diverging waves into a deeply locked self-focusing regime. The model also demonstrates remarkable resilience against thermodynamic effects driven by high kinetic thermal diffusion. The increasing local density of the ramp effectively compensates for elevated electron temperatures, maintaining stable waveguiding even in highly dissipative environments (up to 110 eV).Importantly, we found that complete radial electron cavitation acts as a physical saturation mechanism in the extreme relativistic intensity regime. Rather than the non-physical singular beam collapse $(f_0 \to 0)$predicted by standard paraxial models, the total depletion of on-axis electrons freezes any further refractive index steepening. This establishes a rigid structural floor on the minimum waist size $(f_0 \approx 0.38 - 0.4)$, which inherently prevents catastrophic mathematical singularities.Ultimately, these insights translate into experimentally tunable macroscopic parameters such as applied magnetic fields (e.g., ≈500 T via capacitor-coil targets) and tailored density gradients. This provides a stable, self-regulating optical channel essential for optimizing advanced applications like laser-wakefield accelerators and long-distance optical energy transport systems.

Declaration of Competing Interest

The authors declare that they have no known competing financial interests or personal relationships that could have appeared to influence the work reported in this paper.

Data availability

No data was used for the research described in the article.

References

[1] D. Strickland, G. Mourou, Compression of amplified chirped optical pulses, Opt. Commun. 56 (3) (1985) 219–221, https://doi.org/10.1016/0030-4018(85)90120-8.
[2] R.W. Boyd. Nonlinear Optics, 4th ed., Academic Press, 2020. https://www.sciencedirect.com/book/9780128110027/nonlinear-optics.
[3] R.Y. Chiao, E. Garmire, C.H. Townes, Self-trapping of optical beams, Phys. Rev. Lett. 13 (15) (1964) 479–482, https://doi.org/10.1103/PhysRevLett.13.479.
[4] S.A. Akhmanov, A.P. Sukhorukov, R.V. Khokhlov, Self-focusing and diffraction of light in a nonlinear medium, Sov. Phys. Uspekhi 10 (5) (1968) 609–636, https://doi.org/10.1070/PU1968v010n05ABEH005849.
[5] D.N. Gupta, H. Suk, Relativistic self-focusing of an intense laser beam in a plasma with a density ramp, J. Appl. Phys. 100 (8) (2006) 083101, https://doi.org/10.1063/1.2357644.
[6] E. Esarey, C.B. Schroeder, W.P. Leemans, Physics of laser-driven plasma-based electron accelerators, Rev. Mod. Phys. 81 (3) (2009) 1229–1285, https://doi.org/10.1103/RevModPhys.81.1229.
[7] D. Umstadter, Relativistic laser-plasma interactions, J. Phys. D Appl. Phys. 36 (8) (2003) R151, https://doi.org/10.1088/0022-3727/36/8/202.
[8] P. Sprangle, C.M. Tang, E. Esarey, Relativistic self-focusing of short-pulse radiation beams in plasmas, IEEE Trans. Plasma Sci. 15 (2) (1987) 145–153, https://doi.org/10.1109/TPS.1987.4316677.
[9] A.A. Hassan, A.K.H. Dagher, M.B. Hassan, The self-focusing of hollow gaussian laser beam in magnetized plasma with transverse magnetic field by operating relativistic nonlinearity, J. Opt. 53 (2024) 1963–1970, https://doi.org/10.1007/s12596-024-01842-w.
[10] A.G. Litvak, Finite-amplitude wave beams in a magnetoactive plasma, Sov. Phys. JETP 30 (2) (1969) 344–347.
[11] F.F. Chen. Introduction to Plasma Physics and Controlled Fusion, 3rd ed., Springer, 2016 https://doi.org/10.1007/978-3-319-22309-4.
[12] C.S. Liu, V.K. Tripathi, Interaction of electromagnetic waves with electron beams and plasmas, World Sci. (1994), https://doi.org/10.1142/2070.
[13] P. Jha, P. Kumar, G. Raj, A.K. Upadhyaya, Relativistic self-focusing of right circularly polarized laser beam in a magnetized plasma, Phys. Plasmas 12 (12) (2005) 123104, https://doi.org/10.1063/1.2141932.
[14] C.E. Max, J. Arons, A.B. Langdon, Self-modulation and self-focusing of electromagnetic waves in plasmas, Phys. Rev. Lett. 33 (4) (1974) 209–212, https://doi.org/10.1103/PhysRevLett.33.209.
[15] A.A. Hassan, A.K.H. Dagher, M.B. Hassan, Excitation of a terahertz field by relativistic interaction of a hollow Gaussian laser beam (HGLB) in the transverse magnetized plasma, Indian. J. Phys. 99 (8) (2025) 3095–3102, https://doi.org/10.1007/s12648-024-03512-w.
[16] T. Kurki-Suonio, P.J. Morrison, T. Tajima, Self-focusing of an optical beam in a plasma, Phys. Rev. A 40 (6) (1989) 3230–3239, https://doi.org/10.1103/PhysRevA.40.3230.
[17] P. Jha, R.K. Mishra, A.K. Upadhyaya, G. Raj, Relativistic self-focusing of a circularly polarized laser beam in a magnetized plasma, Phys. Plasmas 13 (10) (2006) 103102, https://doi.org/10.1063/1.2357715.
[18] T. Tajima, J.M. Dawson, Laser electron accelerator, Phys. Rev. Lett. 43 (4) (1979) 267–270, https://doi.org/10.1103/PhysRevLett.43.267.
[19] W.B. Mori, The physics of the surfing routing in laser plasma accelerators, IEEE J. Quantum Electron. 33 (11) (1997) 1942–1953, https://doi.org/10.1109/3.641309.
[20] D. Bora, P. Kumar, Role of axial density gradients in the self-channeling of intense short pulses, Phys. Plasmas 32 (4) (2025) 043105, https://doi.org/10.1063/5.0201011.
[21] M.S. Sodha, A.K. Ghatak, V.K. Tripathi, Self-focusing of laser beams in plasmas and semiconductors, Progress. Opt. 13 (1976) 169–265. https://ui.adsabs.harvard.edu/link_gateway/1976PrOpt.13.169S/doi:10.1016/S0079-6638(08)70021-0.
[22] L. Bhasin, V.K. Tripathi, Self-focusing of an intense laser beam in a plasma with a density ramp, Phys. Plasmas 16 (10) (2009) 103105, https://doi.org/10.1063/1.3248303.
[23] V.L. Ginzburg, The propagation of electromagnetic waves in plasmas, Pergamon Press, 1970.
[24] G. Sun, E. Ott, Y.C. Lee, P. Guzdar, Self-focusing of short intense pulses in plasmas, Phys. Fluids 30 (2) (1987) 526–532, https://doi.org/10.1063/1.866349.
[25] D.P. Garuchava, I.G. Murusidze, G.I. Suramlishvili, Relativistic ponderomotive self-focusing of a laser beam in a magnetized plasma, Sov. J. Plasma Phys. 16 (1) (1990) 51–55.
[26] N. Kant, M.A. Wani, A. Singh, Self-focusing of an intense short pulse laser in a magnetized plasma with density ramp, Optik 182 (2019) 1056–1061, https://doi.org/10.1016/j.ijleo.2019.02.023.
[27] P. Monot, T. Auguste, L.A. Lompré, G. Mainfray, C. Manus, Focusing limits of a terawatt laser in an underdense plasma, J. Opt. Soc. Am. B 9 (9) (1992) 1579–1584, https://doi.org/10.1364/JOSAB.9.001579.
[28] R. Sadighi-Bonabi, M. Habibi, E. Yazdani, Influence of temperature on relativistic self-focusing of a circularly polarized laser beam in a magnetized plasma, Phys. Plasmas 16 (8) (2009) 083105, https://doi.org/10.1063/1.3194272.
[29] B. Hafizi, A. Ting, P. Sprangle, R.F. Hubbard, Relativistic focusing and ponderomotive channeling of intense laser beams, Phys. Rev. E 62 (3) (2000) 4120–4125, https://doi.org/10.1103/PhysRevE.62.4120.
[30] S.M. Hosseini, F.M. Aghamir, Self-focusing of a circularly polarized laser beam in a magnetized plasma, Phys. Plasmas 18 (1) (2011) 013101, https://doi.org/10.1063/1.3533435.
[31] H.S. Ghotra, Advanced self-focusing of Hermite-cosh Gaussian laser beam in relativistic quantum plasmas, Opt. Commun. (2026) 133438, https://doi.org/10.1016/j.optcom.2026.133438.
[32] H.S. Ghotra, L. Singh, Self-focusing of low order LG laser beam in Gaussian plasma, Laser Phys. Lett. 20 (9) (2023) 096001, https://doi.org/10.1088/1612-202X/ace9ca.
[33] Enhanced terahertz radiation generation using q-Gaussian laser beams in a density rippled plasma, J. Opt. 55 (2026) 3630–3636, https://doi.org/10.1007/s12596-024-02431-7.
[34] H.S. Ghotra, Relativistic and quantum dynamics of Hermite–Gaussian laser beams in graded-density plasmas, Phys. Scr. 101 (33) (2026) 335602, https://doi.org/10.1088/1402-4896/ae980c.
[35] S. Kumar, K. Ali, A. Kumar, et al., Langmuir Wave-Assisted Two-Photon Decay of an Amplitude-Modulated Gaussian Laser Beam in Rippled Density Plasma, Arab. J. Sci. Eng. 50 (2025) 559–570, https://doi.org/10.1007/s13369-024-09234-9.
[36] N. Kant, M.A. Wani, A. Kumar, Self-focusing of Hermite–Gaussian laser beams in plasma under plasma density ramp, Opt. Commun. 285 (21-22) (2012) 4483–4487, https://doi.org/10.1016/j.optcom.2012.05.065.
[37] K. Ali, S. Kumar, S.P. Mishra, et al., Nonlinear absorption of Hermite cosh-Gaussian laser beam in an assembly of cylindrical carbon nanotubes embedded with static magnetic field, Opt. Quant. Electron. 56 (2024) 1405, https://doi.org/10.1007/s11082-024-07344-0.
[38] K. Ali, S. Kumar, A. Kumar, A. Varma, Influence of field optimization property of Hermite cosh-Gaussian laser beam on nonlinear absorption in arrays of vertically aligned cylindrical carbon nanotubes, Radiat. Eff. Defects Solids 180 (11–12) (2025) 1795–1809, https://doi.org/10.1080/10420150.2025.2484740.
[39] S. Kumar, K. Ali, A. Kumar, A. Kumar, A. Varma, Plasma wave-assisted two-photon decay of skew cosh-Gaussian laser beam in a magnetized collisional nanoclustered plasma, Radiat. Eff. Defects Solids 181 (7–8) (2026) 1037–1058, https://doi.org/10.1080/10420150.2025.2576874.
[40] S. Kumar, K. Ali, A. Kumar, A. Kumar, S.P. Mishra, A. Varma, Enhanced anomalous electron heating by nonlinear interaction of plasma wave–aided beat wave of two identical profile laser beams in plasma with density ripple, Fusion. Sci. Technol. (2025) 1–12, https://doi.org/10.1080/15361055.2025.2589015.
[41] S. Kumar, K. Ali, A. Kumar, et al., Excitation of Ion bernstein and ion cyclotron waves by an ion beam in a ripple density plasma, Braz. J. Phys. 56 (2026) 19, https://doi.org/10.1007/s13538-025-01916-5.
[42] K. Ali, S. Kumar, A. Kumar, et al., Effect of ambient magnetic field on surface plasma wave-assisted second harmonics over metal surfaces embedded with carbon nanotubes, Eur. Phys. J. 141 (2026) 902, https://doi.org/10.1140/epjp/s13360-026-08067-9.
[43] K. Ali, S. Kumar, A. Kumar, A. Kumar, A. Varma, Surface plasma wave aided Laguerre–Gaussian laser beam second harmonic generation in arrays of vertically aligned carbon nanotube over metal surface, J. Laser Appl. 37 (3) (2025), https://doi.org/10.2351/7.0001819.

[44] A. Kumar, A. Kumar, S.P. Mishra, et al., Plasma wave aided heating of collisional nanocluster plasma by nonlinear interaction of two high power laser beams, Opt. Quant. Electron. 54 (2022) 753, https://doi.org/10.1007/s11082-022-04206-5.
[45] A. Kumar, S.P. Mishra, A. Kumar, A. Varma, Electron Bernstein wave aided cosh-Gaussian laser beam absorption in plasma, Optik 273 (2023) 170436, https://doi.org/10.1016/j.ijleo.2022.170436.
[46] A. Kumar, S.P. Mishra, S. Kumar, et al., Excitation of electron Bernstein wave by nonlinear interaction of two copropagating Hermite–Gaussian laser beams in collisional plasma with static magnetic field, Opt. Quant. Electron. 55 (2023) 598, https://doi.org/10.1007/s11082-023-04883-w.
[47] A. Varma, S.P. Mishra, A. Kumar, et al., Nonlinear absorption of Cosh-Gaussian laser beam in arrays of vertically aligned carbon nanotube, Plasmonics 19 (2024) 505–521, https://doi.org/10.1007/s11468-023-02001-w.
[48] A. Varma, S.P. Mishra, A. Kumar, S. Kumar, A. Kumar, Electron plasma wave excitation by two co-propagating super-Gaussian laser beams in collisional nanocluster Plasma, J. Theor. Appl. Phys. 17 (5) (2023), https://doi.org/10.57647/J.JTAP.2023.1705.54.
[49] A. Varma, S.P. Mishra, A. Kumar, et al., Laguerre-Gaussian laser beam second harmonic generation in arrays of vertically aligned carbon nanotube, Plasmonics 20 (2025) 305–324, https://doi.org/10.1007/s11468-024-02284-7.
[50] A. Varma, S.P. Mishra, A. Kumar, et al., Third harmonic generation of cosh-Gaussian laser beam in arrays of vertically aligned carbon nanotube, Opt. Quant. Electron. 56 (2024) 905, https://doi.org/10.1007/s11082-024-06839-0.
[51] A. Varma, S.P. Mishra, A. Kumar, A. Kumar, Electron Bernstein wave aided Hermite cosh-Gaussian laser beam absorption in collisional plasma, Laser Phys. Lett. 20 (7) (2023) 076001, https://doi.org/10.1088/1612-202X/acd4ab.
[52] M.K. Vishwakarma, S.P. Mishra, A. Kumar, A. Kumar, A. Varma, Excitation of a large amplitude electrostatic wave by counterpropagation of two laser beams in spherical nanoparticles, Radiat. Eff. Defects Solids 181 (7–8) (2026) 1227–1247, https://doi.org/10.1080/10420150.2025.2581584.
[53] W.L. Kruer, The physics of laser plasma interactions, CRC Press, 2003.
[54] T.H. Stix, Waves in Plasmas, American Institute of Physics, 1992.
[55] B. Quesnel, P. Mora, Theory and simulation of the interaction of ultra-intense laser pulses with electrons in vacuum, Phys. Rev. E 58 (3) (1998) 3719–3732, https://doi.org/10.1103/PhysRevE.58.3719.
[56] P. Mora, Plasma expansion into a vacuum, Phys. Rev. Lett. 90 (18) (2003) 185002, https://doi.org/10.1103/PhysRevLett.90.185002.
[57] A. Pitale, Self-focusing of electromagnetic waves in a magnetoplasma, Phys. Fluids 20 (9) (1977) 1528–1531, https://doi.org/10.1063/1.862035.
[58] G. Schmidt, W. Horton, Ponderomotive forces in collisionless plasmas, Comments Plasma Phys. Control. Fusion. 9 (3) (1985) 85–98.
[59] P. Gibbon, Short pulse laser interactions with matter, World Scientific Publishing, 2005, https://doi.org/10.1142/p114.
[60] Y.B. Fainberg, Acceleration of particles in plasmas, Sov. Phys. Uspekhi 10 (6) (1968) 750–768.
[61] A. Upadhyay, V.K. Tripathi, Excitation of plasma waves by ponderomotive force of a circularly polarized laser, J. Appl. Phys. 135 (12) (2024) 123301, https://doi.org/10.1063/5.0192837.
[62] G.P. Agrawal. Nonlinear Fiber Optics, 5th ed., Academic Press, 2012 https://doi.org/10.1016/C2011-0-00045-5.
[63] D. Subbarao, R. Uma, Paraxial theory of self-focusing, Phys. Plasmas 8 (12) (2001) 5364–5373, https://doi.org/10.1063/1.1416886.
[64] Y.R. Shen, The principles of nonlinear optics, John Wiley & Sons, 1984.
[65] M. Lax, W.H. Louisell, W.B. McKnight, From maxwell to paraxial wave optics, Phys. Rev. A 11 (4) (1975) 1365–1370.
[66] V.I. Talanov, Self-focusing of wave beams in nonlinear media, JETP Lett. 2 (5) (1965) 138–141.
[67] A.A. Hassan, A.K.H. Dagher, M.B. Hassan, Transverse magnetic field impact on terahertz wave stimulation in relativistic interaction between hollow gaussian laser beam and collisionless plasma, J. Opt. (2025), https://doi.org/10.1007/s12596-025-02545-6.
[68] X. Liu, D. Umstadter, Competition between ponderomotive and thermal self-focusing in plasmas, Phys. Rev. Lett. 69 (13) (1992) 1935–1938, https://doi.org/10.1103/PhysRevLett.69.1935.
[69] M. Kaur, A.K. Sharma, Self focusing of a right circularly polarized laser beam in a cold magnetized plasma, Optik 122 (20) (2011) 1813–1816, https://doi.org/10.1016/j.ijleo.2010.11.020.
[70] M.D. Feit, J.A. Fleck, Beam nonparaxiality, filament formation, and beam breakup in the self-focusing of optical beams, J. Opt. Soc. Am. B 5 (3) (1988) 633–640, https://doi.org/10.1364/JOSAB.5.000633.
[71] A.A. Hassan, N. Hasheem, Studying the fluorescence and absorption parameters of Er:YAG laser using Judd-Oflet model, AIP Conf. Proc. 3264 (2025) 020006, https://doi.org/10.1063/5.0258527.
[72] W. Koechner. Solid-State Laser Engineering, 6th ed., Springer, 2006 https://doi.org/10.1007/0-387-29338-8.
[73] W.H. Press, S.A. Teukolsky, W.T. Vetterling, B.P. Flannery. Numerical Recipes: The Art of Scientific Computing, 3rd ed., Cambridge University Press, 2007.
[74] J.C. Butcher. Numerical Methods for Ordinary Differential Equations, 3rd ed., John Wiley & Sons, 2016 https://doi.org/10.1002/9781119121534.
[75] E. Esarey, P. Sprangle, J. Krall, A. Ting, Overview of plasma-based accelerator concepts, IEEE Trans. Plasma Sci. 24 (2) (1996) 252–288, https://doi.org/10.1109/27.509991.
[76] C.S. Liu, V.K. Tripathi, Interaction of electromagnetic waves with electron beams and plasmas, World Scientific, 1994.
[77] G.Z. Sun, E. Ott, Y.C. Lee, P. Guzdar, Self-focusing of short intense pulses in plasmas, Phys. Fluids 30 (2) (1987) 526–532, https://doi.org/10.1063/1.866349.
[78] B. Hafizi, A. Ting, P. Sprangle, R.F. Hubbard, Relativistic focusing and ponderomotive channeling of intense laser beams in strongly ionized plasmas, Phys. Rev. E 62 (3) (2000) 4120, https://doi.org/10.1103/PhysRevE.62.4120.